

pubs.acs.org/JPCC Article

Coupled 2D Semiconductor—Molecular Excitons with Enhanced Raman Scattering

Christine Muccianti, Sara L. Zachritz, Angel Garlant, Calley N. Eads, Bekele H. Badada, Adam Alfrey, Michael R. Koehler, David G. Mandrus, Rolf Binder, Brian J. LeRoy, Oliver L.A. Monti, and John R. Schaibley*



Cite This: J. Phys. Chem. C 2020, 124, 27637-27644



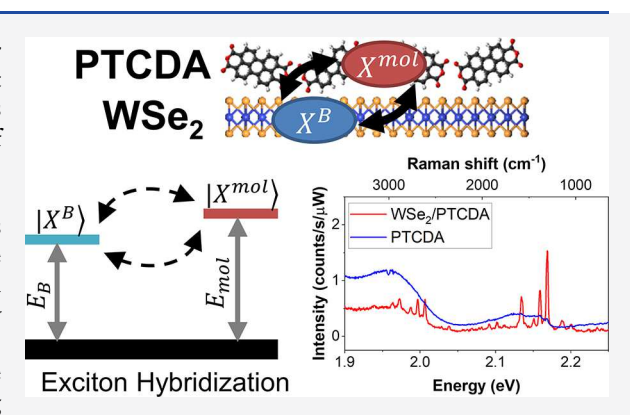
ACCESS

Metrics & More

Article Recommendations

s Supporting Information

ABSTRACT: Two-dimensional (2D) material—organic interfaces offer a platform to realize hybrid materials with tunable optical properties that are determined by the interactions between the disparate materials. This is particularly attractive for tailoring the optoelectronic properties of semiconducting monolayer transition metal dichalcogenides (TMDs). Here, we demonstrate evidence of coupled 2D semiconductor—molecular excitons with enhanced optical properties, which results from the atomically thin heterojunction. Specifically, we investigate the hybridization of the 2.16 eV WSe₂ B exciton with the 2.20 eV transition of perylene-3,4,9,10-tetracarboxylic dianhydride (PTCDA), observed by enhanced resonant Raman scattering by the PTCDA vibrational modes, with enhancements by a factor of nearly 20. The effect can be understood from a coupled oscillator model in which the strong absorption resonance of the WSe₂ monolayer increases the Raman



scattering efficiency of the PTCDA. The Raman enhancement diminishes with increasing WSe_2 thickness, which is attributed to a reflectivity effect that reduces the intensity at the surface. The proposed hybridization effect may lead to new investigations into the nature of coupled excitons in atomically thin junctions.

■ INTRODUCTION

Heterostructures of two-dimensional (2D) materials, where layers of isolated van der Waals materials are brought together, can give rise to novel states of matter. In such structures, interlayer interactions may give rise to unconventional superconducting phases, e.g., in bilayer graphene, and moiré-trapped excitons in transition metal dichalcogenide (TMD) heterostructures.^{2–4} The combination of 2D materials with organic semiconductors is rare in comparison. Studies thus far have focused on using organic molecules as dopants or to drive charge separation and free carrier generation in optoelectronic devices.⁵⁻⁹ Against the backdrop of creating ultraflexible electronic devices, such hybrid 2D semiconductor, organic heterostructures offer considerable potential to tailor electronic properties, and novel states of matter may be anticipated. 10 Hybrid organic-inorganic constructs, e.g., with oxides have been shown to enhance light emission yields significantly and to potentially cause electronic phase transitions near the interface. 11,12

Hybridized excitons in organic—inorganic heterostructures can provide tunability between the properties of the constituent excitons. In 2D organic—inorganic quantum well systems, it is predicted that a hybrid exciton combines the large oscillator strength of the organic Frenkel exciton and the large

nonlinear susceptibility of the inorganic Wannier excitons. 13,14 Several studies have shown experimental evidence of weak exciton hybridization through efficient energy transfer. Due to the dependence on the thickness of the barrier separating the organic layer from the quantum well, it was concluded that the energy transfer was mediated by dipole-dipole Förster coupling. 15-17 Strong excitonic state mixing for an organicinorganic quantum well heterostructure was demonstrated by measuring the energy branch splitting for polaritons in an optical microcavity. 18 Outside of the cavity, strong coupling can only come about when the barrier between the organic layer and well is thin and the exciton wavefunctions overlap. 14,15 This criterion can be achieved by replacing the quantum well with a 2D semiconductor. For instance, a recent study in MoSe₂/WS₂ heterostructures demonstrates strong mixing between the interlayer exciton and the MoSe₂ exciton due to the large wavefunction overlap, evidenced by energy

Received: July 17, 2020
Revised: November 21, 2020
Published: December 7, 2020





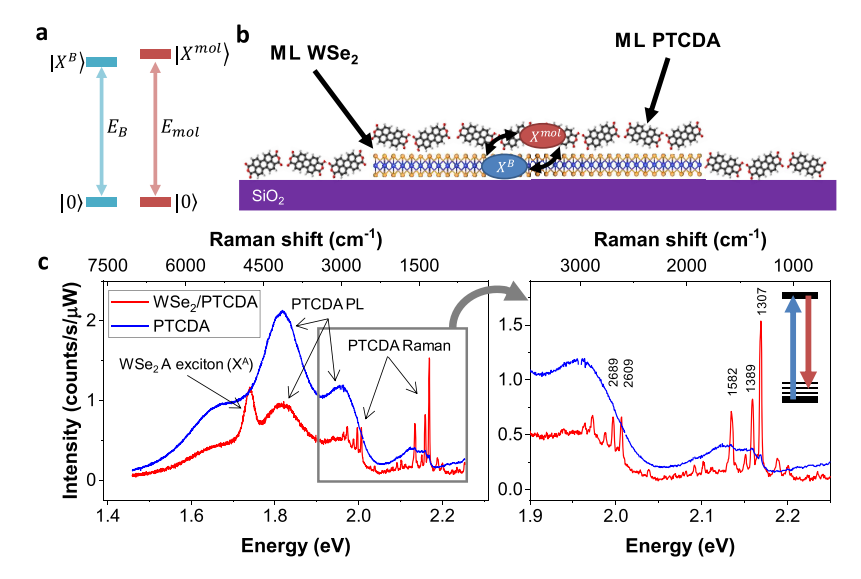


Figure 1. (a) Energy of the B exciton (X^B) and the Frenkel exciton in PTCDA (X^{mol}) are nearly degenerate with values of $E_B = 2.16$ eV and $E_{mol} = 2.20$ eV. (b) Diagram of the PTCDA/WSe₂ heterostructure. ML WSe₂ was exfoliated onto a SiO₂ wafer and then ML PTCDA was thermally evaporated on top. This left areas of the PTCDA/WSe₂ heterostructure as well as areas of ML PTCDA directly on SiO₂. Shown in the heterostructure region is the interaction between the excitons of the two materials. (c) Spectra showing the enhancement of Raman scattering of PTCDA on top of WSe₂. Measurements were taken on the heterostructure (red) and just off the heterostructure (blue). The calculated Raman EFs are 14.8–19.1. The inset shows a schematic of resonant Raman scattering in which excitation on an electron transition with a strong optical transition dipole moment yields a greater Raman cross-section. The blue arrow depicts the excitation photon, and the red arrow depicts the Raman scattered photon.

splitting and sharing of oscillator strength.¹⁹ In the present work, we explore how the combination of 2D inorganic and organic semiconductor layers results in new types of hybridized excitons, observed as enhanced Raman scattering in the heterostructure. For this study, we investigate exciton hybridization with monolayer (ML) films of perylene-3,4,9,10tetracarboxylic dianhydride (PTCDA) on ML and few-layer WSe2. ML WSe2 is an outstanding 2D TMD semiconductor which is known to host strongly bound excitons and trions^{20,21} and has been previously used in the study of interlayer excitons in bilayer heterostructures.²²⁻²⁵ PTCDA is a prototypical organic semiconductor that forms ordered structures on 2D materials^{26,27} with a strong excitonic 0-0 absorption. The PTCDA Frenkel exciton resonance (X^{mol}) at 2.20 eV and the WSe₂ B exciton resonance (X^B) at 2.16 eV²⁰ are nearly degenerate, shown in Figure 1a, and provide the potential for strong exciton mixing, shown in Figure 1b.

METHODS

Sample Preparation. Bulk WSe₂ was mechanically exfoliated onto 290 nm SiO₂/Si wafer chips, and ML flakes were identified using optical microscopy and confirmed using photoluminescence (PL) measurements. Triple-sublimated PTCDA was evaporated using a Knudsen cell under ultrahigh vacuum conditions to deposit an average film thickness of 1 ML over the entire chip. This produced both the hybrid heterostructure and areas with only PTCDA on bare SiO₂/Si, as shown in Figure 1b. To study the effect of doping on the heterostructure, samples were fabricated with an electrical contact to the WSe₂ layer by electron beam lithography and thermal evaporation of 5 nm Cr/30 nm Au prior to deposition of PTCDA.

Optical Measurements. All PL and Raman measurements were performed on a sample in a vacuum cryostat cooled to \sim 3.5 K unless otherwise noted. The excitation source was

focused to a spot size of about 1 μ m using a 40×, NA = 0.6 objective, and the emission was recorded with a single-grating spectrometer equipped with a cooled CCD camera.

■ RESULTS AND DISCUSSION

Figure 1c shows the difference of the emission spectrum between the heterostructure (PTCDA/WSe₂/SiO₂) and pure PTCDA on SiO₂, acquired with an excitation energy of 2.33 eV at \sim 3.5 K. The inset of Figure 1c shows the strongly enhanced resonant Raman scattering on the heterostructure, which functions as a fingerprint of exciton hybridization, as discussed below. On the heterostructure, we see that (1) the Raman modes of the PTCDA are enhanced, (2) Raman overtones and combination bands of the PTCDA are also strongly enhanced, (3) the PTCDA PL is partially quenched, (4) the A exciton of the WSe₂ (X^A) is partially quenched, ²⁰ and (5) the charged and defect excitons of WSe2 are completely quenched (see Supporting Information Figure S1). In order to quantify the Raman enhancement, we calculate an enhancement factor (EF) by taking the ratio between the intensities of a Raman peak both on and off the heterostructure, $EF = I_{HS}/I_{off}$. These intensities were found by integrating the signal over the peak and subtracting the contribution from the broad PL features. The EFs for the three prominent first-order modes are 19.1 for 1307 cm⁻¹, 14.8 for 1389 cm⁻¹, and 16.1 for 1582 cm⁻¹, respectively. This variation in EF is assumed to be random as no trend was found in their relative values for different excitation energies. The EFs for the overtones and combination bands cannot be calculated because they are too weak in the spectrum of the pure PTCDA film; however, all are of A_g symmetry, ^{28,29} consistent with the selection rules in the theoretical framework by Albrecht. 30 Temperature- and power-dependent spectra are shown in the Supporting Information (Figure S2).

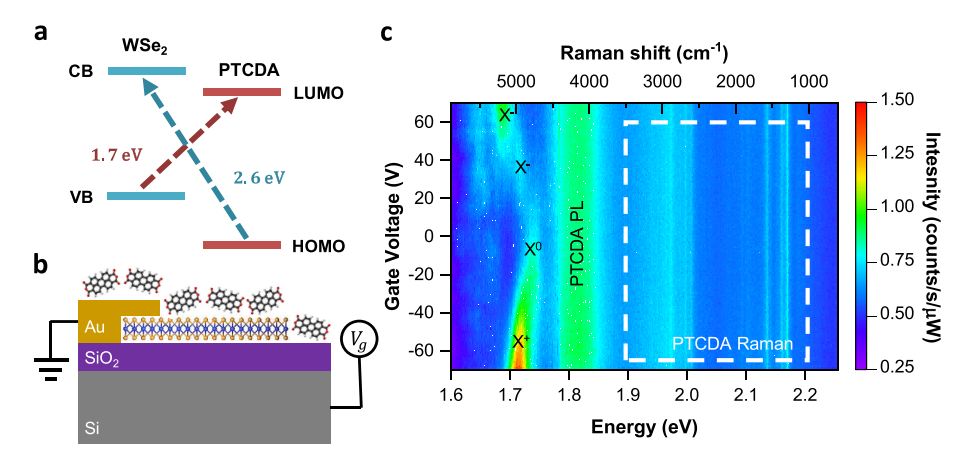


Figure 2. (a) Predicted type-II energy level alignment of PTCDA on ML WSe₂. The predicted charge transfer transitions are shown as dashed arrows. We note that these resonances are far detuned from the excitation energy (2.33 eV) and likely do not contribute to the enhanced Raman scattering. (b) Schematic of the field-effect device. The sample can be electrostatically doped by grounding an electrical contact on ML WSe₂ and applying a voltage to the doped Si back gate. PTCDA was deposited after the fabrication of the electrical contact. (c) Gate-dependent spectra of the heterostructure. While the presence of WSe₂ exciton species changes with doping, the Raman intensity and the PTCDA PL intensity are constant.

A recent body of work suggests that these effects might lie in charge-transfer interactions between the molecule and the ML substrate. In the pioneering work measuring Raman enhancement on graphene substrates, 31–33 it is argued that the charge transfer effect is determined by two different interface properties: the alignment of the highest occupied molecular orbital (HOMO) and lowest unoccupied molecular orbital (LUMO) with the graphene Fermi level, as well as symmetry matching between the molecular structure and the graphene lattice, which enhances the coupling. If the band alignment creates a charge transfer transition near the excitation energy, resonant Raman enhancement may be observed, and symmetry matching enables this charge transfer. Similar resonant Raman effects are predicted to occur in semiconductors for charge transfer states between the molecule and substrate (e.g., valence band VB-LUMO and HOMO-conduction band CB). Though surface-enhanced Raman scattering on ML semiconducting TMD substrates has not been extensively studied, there are reports linking the effect to such charge transfer processes. Studies by Ling et al.³² of copper phthalocyanine (CuPc) on ML MoS₂ and by Muehlethaler et al.³⁵ of 4mercaptopyridine (4-MPy) on ML MoS2 found enhancement upon excitation near a charge transfer resonance. A connection between charge transfer and Raman enhancement has also been demonstrated by Lee et al.³⁶ by constructing phototransistor devices of Rhodamine 6G (R6G) on ML MoS2, ML WSe₂, or graphene and simultaneously measuring the Raman enhancement and the current induced by charge transfer. Amsterdam et al.³⁷ measured various metallophthalocyanine (MPc) molecules on ML MoS₂ which exhibited Raman enhancement correlated with the energies of the molecular transition metal d-orbitals: The more isoenergetic the MPc dorbitals are to the MoS₂ valence band, the more the electronic states will mix, increasing the rate of charge transfer and hence Raman scattering.

To verify that our findings are not of this origin, we first consider the possibility of resonant excitation of or resonant Raman scattering from an interlayer charge transfer transition. Based on the reported ionization energies and electron affinities of PTCDA and WSe₂, ^{27,38–41} the heterojunction is predicted to support a type-II band alignment, though measurement of the complete band structure of the

heterostructure is at present unavailable. Though charge transfer transitions are not observed in our measurements, we estimate the charge transfer resonances to lie at ~1.7 eV (VB to LUMO) and \sim 2.6 eV (HOMO to CB), (Figure 2a). If we assume the linewidth of such a transition to be approximately the same as that of the PTCDA Frenkel exciton (120 meV), 42 then an excitation energy of 2.33 eV exceeds the lowest energy charge transfer resonance by more than ~0.5 eV. We note that this estimate neglects the binding energy of an interlayer exciton; however, we expect any interlayer exciton binding energy to be less than 200 meV based on previous reports of MoSe₂/WSe₂ heterostructures.³⁸ Furthermore, an interface dipole may change the alignment somewhat, but this typically increases the band offsets for such heterostructures, pushing both resonances further away from 2.33 eV. The contribution of interlayer charge transfer bands to the observed Raman enhancement seems, therefore, rather unlikely.

We test this by investigating the dependence of the Raman EF on the sample charge density since a charge transfer mechanism would be sensitive to changes in the Fermi level.³¹ We fabricated field-effect devices to electrostatically dope the WSe₂ layer. A schematic of the device is shown in Figure 2b. A voltage was then applied to the Si back gate and spectra were measured as a function of the applied back gate bias, shown in Figure 2c. We swept the bias from -70 V to +70 V which corresponds to doping densities of $\pm 5.0 \times 10^{12}$ cm⁻². The PL from the WSe2 layer shifts as expected with doping between the neutral and charged exciton species, 20 while there is no apparent change of the Raman features nor their intensity with doping. This supports our estimates of band alignment and charge transfer resonances and suggests that the origin of the Raman enhancement must be found elsewhere. Dopingdependent spectra on an additional sample are shown in Supporting Information Figure S3.

Another possible mechanism of enhanced Raman scattering, found in the work of Morton and Jensen, ⁴³ is the hybridization of electronic states between the molecule and TMD substrate. We do not believe that our results are consistent with this mechanism for several reasons. First, if there was state hybridization between the molecule and the WSe₂ conduction band, we would expect to see Raman enhancement when exciting near the WSe₂ A exciton as well, which is comprised of

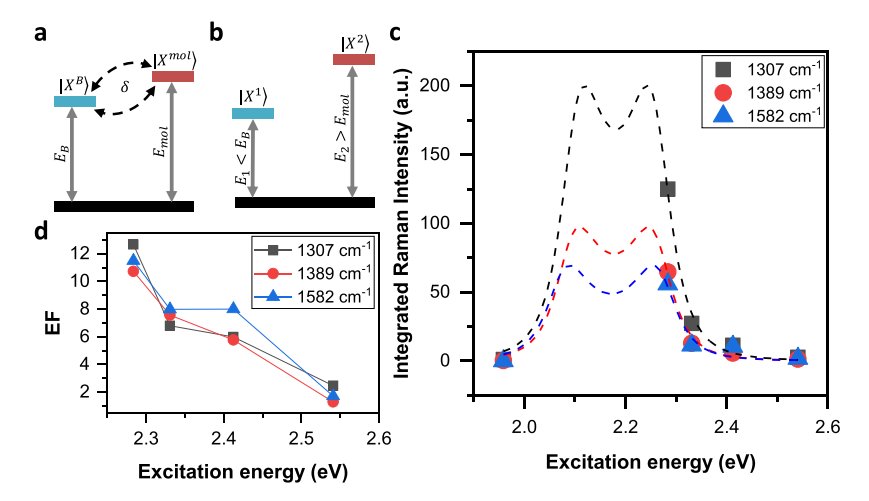


Figure 3. (a) Proposed interaction between X^B and X^{mol} with interaction parameter δ . (b) Creation of new exciton states X^1 and X^2 caused by mixing of X^B and X^{mol} , respectively. The energies are shifted from the uncoupled excitons. (c) Measured (symbols) and simulated (dashed) resonant Raman intensities on the heterostructure with excitation energy. The experimental data are consistent with Raman scattering produced by resonantly exciting a state with energy ~ 2.10 eV which is 60 meV below E_B . (d) EF as a function of excitation energy.

the same conduction band as the B exciton. This was not observed and suggests that the CB does not hybridize with PTCDA states. Second, an analysis based on energy level alignments $^{27,38-41}$ shows that the lower VB of WSe $_2$ and the HOMO of PTCDA are separated by $\sim\!200$ meV. If these states were to hybridize, we would expect to see a shift in PL of $\sim\!100$ meV for both materials, which is not observed, suggesting that the lower VB of WSe $_2$ does not hybridize with the molecular states. Since there is no evidence of band hybridization, we rule out this mechanism of molecule—substrate hybridization.

We instead propose a mechanism involving exciton hybridization giving rise to resonance Raman scattering between coupled states. Resonance Raman scattering is caused by excitation near an electronic transition with an optical transition dipole (inset of Figure 1c). Any mechanism whereby absorption on such a transition is increased, e.g., by changing its energy to be more resonant with the excitation source or by borrowing oscillator strength from another transition, causes increased scattering and thus an enhancement of the Raman scattering. In the case of PTCDA on WSe₂, both aspects are at play: Exciton hybridization shifts the transition into resonance and mixes the character of the WSe2 B exciton and the PTCDA exciton. We model this effect in a simple two-level system where these two excitons, $X^{\rm B}$ and $X^{\rm mol}$, are coupled with an interaction parameter δ as shown in Figure 3a, similar to excitonic mixing invoked previously in hybrid organic/ inorganic quantum well systems with enhanced optical nonlinearities. 13,14,44 The Hamiltonian for this interaction is given by

$$H = \begin{pmatrix} E_{\rm B} & \delta \\ \delta & E_{\rm mol} \end{pmatrix}$$

where $E_{\rm B}=2.16~{\rm eV}$ is the energy of $X^{\rm B}$ (see the Supporting Information) and $E_{\rm mol}=2.20~{\rm eV}$ is the energy of $X^{\rm mol}$. The new exciton states $X^{\rm I}$ and $X^{\rm 2}$ have energy $E_{\rm 1,2}=\frac{1}{2}(E_{\rm B}+E_{\rm mol})\pm\Delta$, where $\Delta=\frac{1}{2}\sqrt{(E_{\rm mol}-E_{\rm B})^2+4\delta^2}$, as shown in Figure 3b.

The resonance shift and wavefunction mixing subsequently alter the resonant Raman scattering cross-section. To model this process, we invoke the standard formalism for Raman scattering with three separate interactions: absorption, scattering, and emission. The probability of absorbing a photon of energy $h\omega_i$ between the ground state $|0\rangle$ and an excited state $|1\rangle$ with energy E_1 is given by Fermi's golden rule, with a transition matrix element $\langle 0 \mid H_E(\omega_i) \mid 1 \rangle$, where $H_E(\omega)$ represents the electron–photon interaction. The probability of emission is given by the matrix element $\langle 1 \mid H_E(\omega_s) \mid 0 \rangle$, where $h\omega_s$ is the energy of the emitted (scattered) photon. Including the electron–phonon interaction with Hamiltonian $H_{\rm ph}$, the probability of a Stokes Raman scattering event off a phonon of energy $E_{\rm ph} = h\omega_i - h\omega_s$ near a resonance then has the form 45

$$P \propto \left| \frac{\langle 0|H_E(\omega_i)|1\rangle\langle 1|H_{ph}|1\rangle\langle 1|H_E(\omega_s)|0\rangle}{(E_1 - h\omega_i - i\Gamma)(E_1 - h\omega_s - i\Gamma)} \right|^2.$$

Here, Γ is a damping factor. From this equation, we see that for a single electronic transition resonance, there are two excitation energies that produce maximum scattering probability: At $h\omega_i = E_1$ (when the excitation is resonant with the electronic transition) and at $h\omega_i = E_1 + E_{\rm ph}$ (when the excitation is resonant with the sum of the electronic and vibrational mode energies).

Our model predicts that hybridization between the molecular exciton and the WSe2 B exciton creates a new hybrid exciton available for resonant Raman scattering with an EF strongly dependent on excitation energy and independent of WSe2 doping. To test this, the Raman intensity was measured using several different excitation energies, as shown in Figure 3c. Due to a limited number of available excitation sources, we were unable to resolve the double peak structure discussed above. However, the intensities show strong enhancement with excitation energy and fall on a resonance curve that is well described by the exciton hybridization model and its effect on resonant Raman scattering. For each Raman mode, the Hamiltonian matrix elements were assumed to have no excitation energy dependence, $E_{\rm ph}$ was fixed, and Γ was independently measured for the $X^{\rm B}$ absorption (see Supporting Information Figure S4). This yields an average value E_1 for the hybrid exciton of 2.095 \pm 0.011 eV, which is well below $E_{\rm B}$ (2.16 eV). This is predicted and consistent with the exciton hybridization model. The corresponding coupling strength and energy offset are $\delta = 77$ meV and $\Delta = 80$ meV, respectively. Furthermore, as predicted by the exciton hybridization model, the EF is mostly independent of the specific vibrational mode but has an excitation energy dependence, as shown in Figure 3d. Enhancement due to the E_2 resonance is not discernable in our measurements. We attribute this to X^2 consisting mostly of the PTCDA exciton.

Since the nature of the exciton in few-layer WSe₂ is strongly thickness-dependent, we investigated the dependence of the EF on WSe₂ layer thickness. ML PTCDA was deposited on an exfoliated piece of WSe2 with areas of different layer thicknesses, as shown in the inset of Figure 4. These

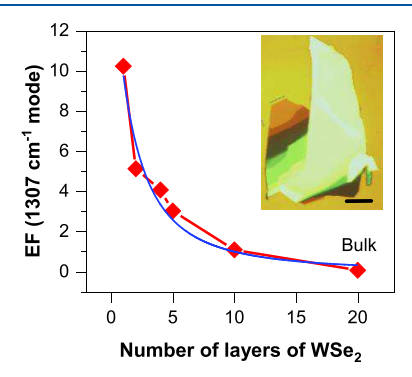


Figure 4. Measured EF (red markers) decreases with the increasing number of WSe2 layers. A model using a transfer matrix approach for the B exciton as a Lorentz oscillator is fit (blue curve) to the data. Inset: an optical image of the multilayered sample used for the measurement (scale bar 5 μ m). More information in the Supporting Information.

thicknesses were determined using atomic force microscopy (see Supporting Information Figure S5). Figure 4 shows that the EF of the 1307 cm⁻¹ Raman line with the number of WSe₂ layers drops sharply between 1 and 2 layers and continues to drop until the bulk limit, which we assume to be reached at 20 ML WSe2. The effect is not due to layer-dependent energy of $X^{\rm B}$ since its energy shifts only by <10 meV, and its absorption coefficient changes by <20% over the first four layers and 30% between the ML and bulk. 46,47 Amsterdam et al. 37 reported a similar layer dependence of CuPc on ML MoS2 and attributed this to increased absorption by the substrate bulk, similar to an argument offered for Raman scattering of CuPc on few-layer graphene by Ling et al.³² Lee et al.³⁶ hypothesized that the layer dependence of R6G on MoS2 or WSe2 was caused by a decrease in the charge transfer rate as the band gap turns from direct to indirect with increasing layer thickness. We investigate this trend by examining the field intensity at the interface using a transfer matrix approach modeling the B exciton as a Lorentz oscillator (for more details, see the Supporting Information). For constant excitation intensity, the intensity at the surface decreases with the number of WSe2 layers, N, with the dependence

$$I \propto \frac{\gamma^2}{(\gamma + N\Gamma_{rad})^2}$$

where $\Gamma_{\rm rad}$ is the radiative decay rate and γ contains the nonradiative decay and dephasing rates. The fit to our data, shown by the solid blue curve in Figure 4, produces $\Gamma_{\rm rad}/\gamma$ = 0.31 ± 0.08 . The dominant nonradiative decay path is relaxation from the B to A exciton states. In MoS_2 , this is found to be ~ 1 ps. ⁴⁸ For a radiative lifetime of several ps, ^{49,50} this ratio is consistent with B exciton dynamics and thus the B exciton's involvement in the enhanced Raman scattering.

We note that it may be possible for the reduction in the EF to be related to the reduced wavefunction overlap, consistent with results on organic/inorganic quantum well systems.¹³ Though the A exciton wavefunction is localized to one single layer, 51 the B exciton may have finite hopping with the excited A exciton state from a neighboring layer, making its wavefunction less localized than the A exciton. However, quantitative investigation of this hopping is currently lacking.

To test the validity and generality of our observations, we also measured enhancement of Raman scattering on ML MoSe₂ and graphene and found EFs of 5.3-12.9 and 4.8-13.0, respectively (see Supporting Information Figure S7). Both ML MoSe₂ and graphene have similar absorption coefficients as WSe₂ at 2.33 eV excitation. 46,47,52-55 Transitions of energy $E_{\rm mol}$ in both MoSe₂ and graphene are not to discrete exciton states but rather to continuum states. These transitions can, however, still mix with X^{mol} by the same mechanism as in WSe2, and the resulting EFs reflect therefore the degree of hybridization at the 2D substrate-organic interface. We note that our measured EFs for PTCDA on WSe2 MoSe2 and graphene are similar to previous studies, shown in Table 1, which could motivate new interpretations of previous results.

Table 1. Comparison of Raman EFs on 2D Materials

| study | molecule | 2D substrate | EFs |
|--------------------------------|----------------------|--------------|------------|
| this study | PTCDA | WSe_2 | Up to 19.1 |
| | PTCDA | $MoSe_2$ | 5.3-12.9 |
| | PTCDA | graphene | 4.8 - 13.0 |
| Amsterdam et al. ³⁴ | CuPc | MoS_2 | Up to 25.8 |
| | NiPc | MoS_2 | Up to 23.4 |
| | CuPc | MoS_2 | Up to 9.2 |
| | ZnPc | MoS_2 | Up to 4.9 |
| | H2Pc | MoS_2 | Up to 1.6 |
| Huang et al. ³⁰ | CuPc | graphene | 11.6-47.3 |
| | F ₁₆ CuPc | graphene | 2.7 - 6.2 |
| | PTCDA | graphene | 3.9-8.3 |
| Ling et al. ²⁹ | CuPc | graphene | 5.2-63.5 |
| | CuPc | hBN | 6.9-29.5 |
| | CuPc | MoS_2 | Up to 16 |
| | | | |

CONCLUSIONS

In summary, we have demonstrated that Raman enhancement in PTCDA/WSe2 heterostructures can be attributed to the hybridization of nearly degenerate PTCDA and WSe2 B excitons. These excitons are nearly resonant and interact strongly, resulting in an increased absorption coefficient, activation of resonant Raman scattering, and thus enhanced Raman scattering. This picture is consistent with the measured dependence of the EF on excitation energy and WSe2 layer thickness, and with enhanced Raman scattering from PTCDA on ML MoSe₂ and graphene where the coupling interaction takes place between the PTCDA Frenkel exciton and transitions to continuum states in the substrate at this energy. Further understanding of this exciton hybridization mechanism can be achieved by studies on other exciton-matched molecule-TMD pairs as well as more extensive measurements of the EF dependence on excitation energy. The present work elucidates how excitons in 2D and organic semiconductors can hybridize, giving rise to novel optical effects. We anticipate that this work will motivate future studies which seek to tailor the organic—inorganic interlayer interactions and create novel electronic phases in TMDs, e.g., through resonant exciton effects as well as wavefunction engineering.

ASSOCIATED CONTENT

Supporting Information

The Supporting Information is available free of charge at https://pubs.acs.org/doi/10.1021/acs.jpcc.0c06544.

Additional spectra characterizing the Raman enhancement effect and the heterostructure's constituent materials; doping-dependent measurements of a heterostructure with reverse construction; characterization of the multilayer sample; determination of thickness-dependent field intensity at the interface; and spectra showing the enhancement effect on other materials (PDF)

AUTHOR INFORMATION

Corresponding Author

John R. Schaibley — Department of Physics, University of Arizona, Tucson, Arizona 85721, United States; Email: johnschaibley@email.arizona.edu

Authors

Christine Muccianti — Department of Physics, University of Arizona, Tucson, Arizona 85721, United States;
orcid.org/0000-0001-7265-9822

Sara L. Zachritz – Department of Chemistry and Biochemistry, University of Arizona, Tucson, Arizona 85721, United States

Angel Garlant – Department of Physics and Department of Chemistry and Biochemistry, University of Arizona, Tucson, Arizona 85721, United States

Calley N. Eads – Department of Chemistry and Biochemistry, University of Arizona, Tucson, Arizona 85721, United States

Bekele H. Badada – Department of Physics, University of Arizona, Tucson, Arizona 85721, United States

Adam Alfrey – Department of Physics, University of Arizona, Tucson, Arizona 85721, United States

Michael R. Koehler – Department of Materials Science and Engineering, University of Tennessee, Knoxville, Tennessee 37996, United States

David G. Mandrus — Department of Materials Science and Engineering and Department of Physics and Astronomy, University of Tennessee, Knoxville, Tennessee 37996, United States; Materials Science and Technology Division, Oak Ridge National Laboratory, Oak Ridge, Tennessee 37831, United States; orcid.org/0000-0003-3616-7104

Rolf Binder – Department of Physics and James C. Wyant College of Optical Sciences, University of Arizona, Tucson, Arizona 85721, United States

Brian J. LeRoy – Department of Physics, University of Arizona, Tucson, Arizona 85721, United States

Oliver L.A. Monti – Department of Physics and Department of Chemistry and Biochemistry, University of Arizona, Tucson, Arizona 85721, United States

Complete contact information is available at: https://pubs.acs.org/10.1021/acs.jpcc.0c06544

Notes

The authors declare no competing financial interest.

ACKNOWLEDGMENTS

The authors acknowledge useful discussions with Carlo Piermarocchi and Hongyi Yu. This work is mainly supported by the National Science Foundation under Grant No. ECCS-1708562. M.R.K. and D.G.M. acknowledge support from the Gordon and Betty Moore Foundation's EPiQS Initiative through grant GBMF9069. J.R.S. acknowledges support from The Science Foundation of Arizona, Bisgrove Scholars Program (Grant No. BSP 0821-17), AFOSR (Grant Nos. FA9550-17-1-0215, FA9550-18-1-0049, FA9550-18-1-0390), and the National Science Foundation (Grant No. DMR-1838378). R.B. acknowledges support from the National Science Foundation under Grant No. DMR-1839570. B.J.L. acknowledges support from the National Science Foundation under Grant No. ECCS-1607911. AFM images and data were collected in the W.M. Keck Center for Nano-Scale Imaging, Department of Chemistry and Biochemistry, University of Arizona, using equipment supported by the National Science Foundation under Grant No. 1337371.

REFERENCES

- (1) Cao, Y.; Fatemi, V.; Fang, S.; Watanabe, K.; Taniguchi, T.; Kaxiras, E.; Jarillo-Herrero, P. Unconventional Superconductivity in Magic-Angle Graphene Superlattices. *Nature* **2018**, *556*, 43–50.
- (2) Tran, K.; Moody, G.; Wu, F.; Lu, X.; Choi, J.; Kim, K.; Rai, A.; Sanchez, D. A.; Quan, J.; Singh, A.; et al. Evidence for Moiré Excitons in van Der Waals Heterostructures. *Nature* **2019**, *567*, 71–75.
- (3) Seyler, K. L.; Rivera, P.; Yu, H.; Wilson, N. P.; Ray, E. L.; Mandrus, D. G.; Yan, J.; Yao, W.; Xu, X. Signatures of Moiré-Trapped Valley Excitons in MoSe₂/WSe₂ Heterobilayers. *Nature* **2019**, 567, 66–70.
- (4) Jin, C.; Regan, E. C.; Yan, A.; Iqbal Bakti Utama, M.; Wang, D.; Zhao, S.; Qin, Y.; Yang, S.; Zheng, Z.; Shi, S.; et al. Observation of Moiré Excitons in WSe₂/WS₂ Heterostructure Superlattices. *Nature* **2019**, *567*, 76–80.
- (5) Kafle, T. R.; Kattel, B.; Lane, S. D.; Wang, T.; Zhao, H.; Chan, W. L. Charge Transfer Exciton and Spin Flipping at Organic-Transition-Metal Dichalcogenide Interfaces. *ACS Nano* **2017**, *11*, 10184–10192.
- (6) Choi, J.; Zhang, H.; Choi, J. H. Modulating Optoelectronic Properties of Two-Dimensional Transition Metal Dichalcogenide Semiconductors by Photoinduced Charge Transfer. *ACS Nano* **2015**, *10*, 1671–1680.
- (7) Liu, X.; Gu, J.; Ding, K.; Fan, D.; Hu, X.; Tseng, Y.; Lee, Y.; Menon, V.; Forrest, S. R. Photoresponse of an Organic Semi-conductor/Two-Dimensional Transition Metal Dichalcogenide Heterojunction. *Nano Lett.* **2017**, *17*, 3176–3181.
- (8) Bettis Homan, S.; Sangwan, V. K.; Balla, I.; Bergeron, H.; Weiss, E. A.; Hersam, M. C. Ultrafast Exciton Dissociation and Long-Lived Charge Separation in a Photovoltaic Pentacene—MoS₂ van Der Waals Heterojunction. *Nano Lett.* **2016**, *17*, 164–169.
- (9) Huang, Y. L.; Zheng, Y. J.; Song, Z.; Chi, D.; Wee, A. T. S.; Quek, S. Y. The Organic–2D Transition Metal Dichalcogenide Heterointerface. *Chem. Soc. Rev.* **2018**, *47*, 3241–3264.
- (10) Kezilebieke, S.; Dvorak, M.; Ojanen, T.; Liljeroth, P. Coupled Yu–Shiba–Rusinov States in Molecular Dimers on NbSe₂. *Nano Lett.* **2018**, *18*, 2311–2315.
- (11) Schlesinger, R.; Bianchi, F.; Blumstengel, S.; Christodoulou, C.; Ovsyannikov, R.; Kobin, B.; Moudgil, K.; Barlow, S.; Hecht, S.; Marder, S. R.; et al. Efficient Light Emission from Inorganic and Organic Semiconductor Hybrid Structures by Energy-Level Tuning. *Nat. Commun.* **2015**, *6*, 6754.
- (12) Racke, D. A.; Kelly, L. L.; Kim, H.; Schulz, P.; Sigdel, A.; Berry, J. J.; Graham, S.; Nordlund, D.; Monti, O. L. A. Disrupted Attosecond Charge Carrier Delocalization at a Hybrid Organic/Inorganic Semiconductor Interface. *J. Phys. Chem. Lett.* **2015**, *6*, 1935–1941.

- (13) Agranovich, V.; Atanasov, R.; Bassani, F. Hybrid Interface Excitons in Organic-Inorganic Quantum Wells. *Solid State Commun.* **1994**, 92, 295–301.
- (14) Agranovich, V. M.; Basko, D. M.; La Rocca, G. C.; Bassani, F. Excitons and Optical Nonlinearities in Hybrid Organic-Inorganic Nanostructures. *J. Phys. Condens. Matter* **1998**, *10*, 9369–9400.
- (15) Blumstengel, S.; Sadofev, S.; Xu, C.; Puls, J.; Henneberger, F. Converting Wannier into Frenkel Excitons in an Inorganic/Organic Hybrid Semiconductor Nanostructure. *Phys. Rev. Lett.* **2006**, *97*, 8–11
- (16) Heliotis, G.; Itskos, G.; Murray, R.; Dawson, M. D.; Watson, I. M.; Bradley, D. D. C. Hybrid Inorganic/Organic Semiconductor Heterostructures with Efficient Non-Radiative Energy Transfer. *Adv. Mater.* **2006**, *18*, 334–338.
- (17) Specht, J. F.; Verdenhalven, E.; Bieniek, B.; Rinke, P.; Knorr, A.; Richter, M. Theory of Excitation Transfer between Two-Dimensional Semiconductor and Molecular Layers. *Phys. Rev. Appl.* **2018**, *9*, No. 044025.
- (18) Slootsky, M.; Liu, X.; Menon, V. M.; Forrest, S. R. Room Temperature Frenkel-Wannier-Mott Hybridization of Degenerate Excitons in a Strongly Coupled Microcavity. *Phys. Rev. Lett.* **2014**, *112*, 1–5.
- (19) Zhang, L.; Zhang, Z.; Wu, F.; Wang, D.; Gogna, R.; Hou, S.; Watanabe, K.; Taniguchi, T.; Kulkarni, K.; Kuo, T.et al. Moiré Lattice-Induced Formation and Tuning of Hybrid Dipolar Excitons in Twisted WS₂/MoSe₂ Heterobilayers. 2019. http://arxiv.org/abs/1911.10069.
- (20) Jones, A. M.; Yu, H.; Ghimire, N. J.; Wu, S.; Aivazian, G.; Ross, J. S.; Zhao, B.; Yan, J.; Mandrus, D. G.; Xiao, D.; et al. Optical Generation of Excitonic Valley Coherence in Monolayer WSe₂. *Nat. Nanotechnol.* **2013**, *8*, 634–638.
- (21) He, K.; Kumar, N.; Zhao, L.; Wang, Z.; Mak, K. F.; Zhao, H.; Shan, J. Tightly Bound Excitons in Monolayer WSe₂. *Phys. Rev. Lett.* **2014**, *113*, 1–5.
- (22) Rivera, P.; Schaibley, J. R.; Jones, A. M.; Ross, J. S.; Wu, S.; Aivazian, G.; Klement, P.; Seyler, K.; Clark, G.; Ghimire, N. J.; et al. Observation of Long-Lived Interlayer Excitons in Monolayer MoSe₂-WSe₂ Heterostructures. *Nat. Commun.* **2015**, *6*, 4–9.
- (23) Rivera, P.; Seyler, K. L.; Yu, H.; Schaibley, J. R.; Yan, J.; Mandrus, D. G.; Yao, W.; Xu, X. Valley-Polarized Exciton Dynamics in a 2D Semiconductor Heterostructure. *Science* **2016**, *351*, 688–691.
- (24) Nagler, P.; Plechinger, G.; Ballottin, M. V.; Mitioglu, A.; Meier, S.; Paradiso, N.; Strunk, C.; Chernikov, A.; Christianen, P. C. M.; Schüller, C.; et al. Interlayer Exciton Dynamics in a Dichalcogenide Monolayer Heterostructure. 2D Mater. 2017, 4, No. 025112.
- (25) Jauregui, L. A.; Joe, A. Y.; Pistunova, K.; Wild, D. S.; High, A. A.; Zhou, Y.; Scuri, G.; De Greve, K.; Sushko, A.; Yu, C.-H.; et al. Electrical Control of Interlayer Exciton Dynamics in Atomically Thin Heterostructures. *Science* **2019**, *366*, 870–875.
- (26) Martínez-Galera, A. J.; Gómez-Rodríguez, J. M. Structural and Electronic Properties of 3,4,9,10-Perylene Tetracarboxylic Dianhydride on h-BN/Rh (110). *J. Phys. Chem. C* **2019**, 123, 1866–1873.
- (27) Zheng, Y. J.; Huang, Y. L.; Chen, Y.; Zhao, W.; Eda, G.; Spataru, C. D.; Zhang, W.; Chang, Y.; Li, L.; Chi, D.; et al. Heterointerface Screening Effects between Organic Monolayers and Monolayer Transition Metal Dichalcogenides. *ACS Nano* **2016**, *10*, 2476–2484.
- (28) Tenne, D.; Park, S.; Kampen, T.; Das, A.; Scholz, R.; Zahn, D. Single Crystals of the Organic Semiconductor Perylene Tetracarboxylic Dianhydride Studied by Raman Spectroscopy. *Phys. Rev. B-Condens. Matter Mater. Phys.* **2000**, *61*, 14564–14569.
- (29) Kobitski, A. Y.; Salvan, G.; Scholz, R.; Tenne, D.; Kampen, T. U.; Wagner, H. P.; Zahn, D. R. T. Raman Spectroscopy of the PTCDA-Inorganic Semiconductor Interface: Evidence for Charge Transfer. *Appl. Surf. Sci.* **2002**, *190*, 386–389.
- (30) Albrecht, A. C. On the Theory of Raman Intensities. *J. Chem. Phys.* **1961**, 34, 1476–1484.
- (31) Barros, E. B.; Dresselhaus, M. S. Theory of Raman Enhancement by Two-Dimensional Materials: Applications for

- Graphene-Enhanced Raman Spectroscopy. Phys. Rev. B 2014, 90, No. 035443.
- (32) Ling, X.; Fang, W.; Lee, Y. H.; Araujo, P. T.; Zhang, X.; Rodriguez-Nieva, J. F.; Lin, Y.; Zhang, J.; Kong, J.; Dresselhaus, M. S. Raman Enhancement Effect on Two-Dimensional Layered Materials: Graphene, h-BN and MoS₂. *Nano Lett.* **2014**, *14*, 3033–3040.
- (33) Huang, S.; Ling, X.; Liang, L.; Song, Y.; Fang, W.; Zhang, J.; Kong, J.; Meunier, V.; Dresselhaus, M. S. Molecular Selectivity of Graphene-Enhanced Raman Scattering. *Nano Lett.* **2015**, *15*, 2892–2901.
- (34) Lombardi, J. R.; Birke, R. L. Theory of Surface-Enhanced Raman Scattering in Semiconductors. *J. Phys. Chem. C* **2014**, *118*, 11120–11130.
- (35) Muehlethaler, C.; Considine, C. R.; Menon, V.; Lin, W.-C.; Lee, Y.-H.; Lombardi, J. R. Ultrahigh Raman Enhancement on Monolayer MoS₂. ACS Photonics **2016**, *3*, 1164–1169.
- (36) Lee, Y.; Kim, H.; Lee, J.; Yu, S. H.; Hwang, E.; Lee, C.; Ahn, J. H.; Cho, J. H. Enhanced Raman Scattering of Rhodamine 6G Films on Two-Dimensional Transition Metal Dichalcogenides Correlated to Photoinduced Charge Transfer. *Chem. Mater.* **2016**, 28, 180–187.
- (37) Amsterdam, S. H.; Stanev, T. K.; Zhou, Q.; Lou, A. J. T.; Bergeron, H.; Darancet, P.; Hersam, M. C.; Stern, N. P.; Marks, T. J. Electronic Coupling in Metallophthalocyanine-Transition Metal Dichalcogenide Mixed-Dimensional Heterojunctions. *ACS Nano* **2019**, *13*, 4183–4190.
- (38) Wilson, N. R.; Nguyen, P. V.; Seyler, K.; Rivera, P.; Marsden, A. J.; Laker, Z. P. L.; Constantinescu, G. C.; Kandyba, V.; Barinov, A.; Hine, N. D. M.; et al. Determination of Band Offsets, Hybridization, and Exciton Binding in 2D Semiconductor Heterostructures. *Sci. Adv.* 2017, 3, No. e1601832.
- (39) Zhang, Y.; Ugeda, M. M.; Jin, C.; Shi, S.; Bradley, A. J.; Martín-Recio, A.; Ryu, H.; Kim, J.; Tang, S.; Kim, Y.; et al. Electronic Structure, Surface Doping, and Optical Response in Epitaxial WSe₂ Thin Films. *Nano Lett.* **2016**, *16*, 2485–2491.
- (40) Yoshida, H. Principle and Application of Low Energy Inverse Photoemission Spectroscopy: A New Method for Measuring Unoccupied States of Organic Semiconductors. *J. Electron Spectros. Relat. Phenomena* **2015**, 204, 116–124.
- (41) Cao, L.; Wang, Y.; Zhong, J.; Han, Y.; Zhang, W.; Yu, X.; Xu, F.; Qi, D. C.; Wee, A. T. S. Electronic Structure, Chemical Interactions and Molecular Orientations of 3,4,9,10-Perylene-Tetracarboxylic-Dianhydride on TiO₂ (110). *J. Phys. Chem. C* **2011**, 115, 24880–24887.
- (42) Djurišić, A. B.; Fritz, T.; Leo, K. Modeling the Optical Constants of Organic Thin Films: Application to 3,4,9,10-Perylenete-tracarboxylic Dianhydride (PTCDA). *Opt. Commun.* **2000**, *183*, 123–132.
- (43) Morton, S. M.; Jensen, L. Understanding the Molecule—Surface Chemical Coupling in SERS. *J. Am. Chem. Soc.* **2009**, *131*, 4090–4098.
- (44) Agranovich, V. M.; Gartstein, Y. N.; Litinskaya, M. Hybrid Resonant Organic-Inorganic Nanostructures for Optoelectronic Applications. *Chem. Rev.* **2011**, *111*, 5179–5214.
- (45) Yu, P. Y.; Cardona, M. Chapter 7: Optical Properties II. In *Fundamentals of Semiconductors*; Stanley, H. E., Rhodes, W. T., Eds.; Springer: Berlin, Heidelberg, 2010; 345–426.
- (46) Arora, A.; Koperski, M.; Nogajewski, K.; Marcus, J.; Faugeras, C.; Potemski, M. Excitonic Resonances in Thin Films of WSe₂: From Monolayer to Bulk Material. *Nanoscale* **2015**, *7*, 10421–10429.
- (47) Koperski, M.; Molas, M. R.; Arora, A.; Nogajewski, K.; Slobodeniuk, A. O.; Faugeras, C.; Potemski, M. Optical Properties of Atomically Thin Transition Metal Dichalcogenides: Observations and Puzzles. *NANO* **2017**, *6*, 1289–1308.
- (48) Cha, S.; Sung, J. H.; Sim, S.; Park, J.; Heo, H.; Jo, M. H.; Choi, H. 1s-Intraexcitonic Dynamics in Monolayer MoS₂ Probed by Ultrafast Mid-Infrared Spectroscopy. *Nat. Commun.* **2016**, *7*, 10768.
- (49) Korn, T.; Heydrich, S.; Hirmer, M.; Schmutzler, J.; Schller, C. Low-Temperature Photocarrier Dynamics in Monolayer MoS₂. *Appl. Phys. Lett.* **2011**, *99*, 2–5.

- (50) Palummo, M.; Bernardi, M.; Grossman, J. C. Exciton Radiative Lifetimes in Two-Dimensional Transition Metal Dichalcogenides. *Nano Lett.* **2015**, *15*, 2794–2800.
- (51) Zhang, L.; Zunger, A. Evolution of Electronic Structure as a Function of Layer Thickness in Group-VIB Transition Metal Dichalcogenides: Emergence of Localization Prototypes. *Nano Lett.* **2015**, *15*, 949–957.
- (52) Arora, A.; Nogajewski, K.; Molas, M.; Koperski, M.; Potemski, M. Exciton Band Structure in Layered MoSe₂: From a Monolayer to the Bulk Limit. *Nanoscale* **2015**, *7*, 20769–20775.
- (53) Kravets, V. G.; Grigorenko, A. N.; Nair, R. R.; Blake, P.; Anissimova, S.; Novoselov, K. S.; Geim, A. K. Spectroscopic Ellipsometry of Graphene and an Exciton-Shifted van Hove Peak in Absorption. *Phys. Rev. B-Condens. Matter Mater. Phys.* **2010**, *81*, 1–6.
- (54) Mak, K. F.; Shan, J.; Heinz, T. F. Seeing Many-Body Effects in Single- and Few-Layer Graphene: Observation of Two-Dimensional Saddle-Point Excitons. *Phys. Rev. Lett.* **2011**, *106*, No. 046401.
- (55) Nair, R. R.; Blake, P.; Grigorenko, A. N.; Novoselov, K. S.; Booth, T. J.; Stauber, T.; Peres, N. M. R.; Geim, A. K. Fine Structure Constant Defines Visual Transparency of Graphene. *Science* **2008**, 320, 1308–1308.